Measuring the composition-curvature coupling in binary lipid membranes by computer simulations

I. A. Barragán Vidal, C. M. Rosetti, C. Pastorino, and M. Müller

Citation: The Journal of Chemical Physics **141**, 194902 (2014); doi: 10.1063/1.4901203
View online: http://dx.doi.org/10.1063/1.4901203
View Table of Contents: http://scitation.aip.org/content/aip/journal/jcp/141/19?ver=pdfcov
Published by the AIP Publishing

Measuring the composition-curvature coupling in binary lipid membranes by computer simulations

I. A. Barragán Vidal,[1,a)] C. M. Rosetti,[2,b)] C. Pastorino,[3,c)] and M. Müller[1,d)]
[1]*Institut für Theoretische Physik, Georg-August-Universität, Friedrich-Hund-Platz 1, 37077 Göttingen, Germany*
[2]*Centro de Investigaciones en Química Biológica de Córdoba, Departamento de Química Biológica, Facultad de Ciencias Químicas, Universidad Nacional de Córdoba, Ciudad Universitaria, Córdoba, Argentina*
[3]*Departamento de Física de la Materia Condensada, Centro Atómico Constituyentes, CNEA/CONICET, Av. Gral. Paz 1499, 1650 Pcia. de Buenos Aires, Argentina*

(Received 4 August 2014; accepted 27 October 2014; published online 17 November 2014)

The coupling between local composition fluctuations in binary lipid membranes and curvature affects the lateral membrane structure. We propose an efficient method to compute the composition-curvature coupling in molecular simulations and apply it to two coarse-grained membrane models—a minimal, implicit-solvent model and the MARTINI model. Both the weak-curvature behavior that is typical for thermal fluctuations of planar bilayer membranes as well as the strong-curvature regime corresponding to narrow cylindrical membrane tubes are studied by molecular dynamics simulation. The simulation results are analyzed by using a phenomenological model of the thermodynamics of curved, mixed bilayer membranes that accounts for the change of the monolayer area upon bending. Additionally the role of thermodynamic characteristics such as the incompatibility between the two lipid species and asymmetry of composition are investigated. © *2014 AIP Publishing LLC*. [http://dx.doi.org/10.1063/1.4901203]

I. INTRODUCTION

The spontaneous curvature of lipid monolayers and the coupling, λ, between composition and curvature in lipid bilayer membranes has attracted abiding interest because it is important for the lateral organization of membranes.[1] For instance, curvature-composition coupling can give rise to spatially modulated phases or microemulsion-like morphologies[2–5] that resemble "rafts," i.e., domains of phospholipids and cholesterol, whose properties differ from their surrounding. Additionally, the coupling between curvature and composition may also be important for highly curved structures[6] like membrane tubes or transition states that occur in transformation of membrane shapes (e.g., pore formation, fusion, and fission[7,8]). Alternatively, proteins or other membrane inclusions can give rise to high local curvatures that modify the local composition in multi-component membranes.

In this paper we propose to measure the coupling between curvature and composition and the concomitant spontaneous curvature of a monolayer by analyzing the composition difference $\Delta\phi$ between apposing monolayers of curved membranes in molecular simulations. This is an alternative to extracting the spontaneous curvature of a monolayer by the first moment of the pressure profile across a bilayer membrane.[9–11] Both the weak-curvature behavior that is typical for thermal fluctuations of planar bilayer membranes as well as the strong-curvature regime corresponding to narrow cylindrical membrane tubes are studied. The latter gives rise to pronounced composition differences that can be accurately determined.

Our simulation results are analyzed using a phenomenological description of the thermodynamics of curved, mixed bilayer membranes.[1] Several models have been proposed to describe the lateral sorting of lipids and its interplay with membrane curvature in model bilayer mixtures comprised of two or three lipid species.[1,3,12–18] All these models comprises three terms: (i) a curvature dependent term that accounts for the elastic energy, (ii) a composition dependent term describing the free energy of mixing, and (iii) an energetic contribution that couples curvature and composition. Although most of these models explicitly distinguish the composition on each leaflet of the bilayer, few of them consider their difference in curvature. This simplification is valid for bilayers in the absence of strong shape fluctuations or curved surfaces with a radius of curvature that is much larger than the bilayer thickness. However, important contributions to the lateral sorting of lipids may arise when these conditions are not met. In this paper we present a simple phenomenological model that explicitly accounts for the curvature difference, resulting in additional contributions to the free energy of mixing. We employ this model to analyze the strength of the curvature-composition coupling from molecular dynamics simulations under different curvature, composition and incompatibilities between the lipid species.

Our paper is arranged as follows: In Sec. II we provide a brief description of the thermodynamics of a curved, mixed bilayer membrane which is used to analyze the

a)Electronic mail: vidal@theorie.physik.uni-goettingen.de
b)Electronic mail: carla@dqb.fcq.unc.edu.ar
c)Electronic mail: pastor@cnea.gov.ar
d)Electronic mail: mmueller@theorie.physik.uni-goettingen.de

composition difference between the apposing monolayers of curved membranes. We use two coarse-grained simulation models—a minimal, implicit-solvent model[19–21] and the MARTINI model[22]—to study the composition-curvature coupling. Section III presents our simulation results for small and large curvatures and small and large incompatibility between the lipid species. The paper closes with a brief summary and an outlook (Sec. V).

II. BACKGROUND

In this section we present a simple, phenomenological model that describes the thermodynamics of mixing in the two monolayers of the membrane and its coupling to the membrane's curvature. For simplicity we consider a spatially homogeneous cylindrical membrane of thickness t_h, characterized by the curvature, $\mathcal{H} = -1/R$, and the area, A, of its midplane, as shown in Fig. 1. In terms of these, the corresponding curvature and area for the upper and lower monolayers (denoted by subscripts u and l, respectively) are

$$\mathcal{H}_u = \frac{\mathcal{H}}{1 - \frac{t_\mathrm{h}}{2}\mathcal{H}}, \qquad \mathcal{H}_l = \frac{-\mathcal{H}}{1 + \frac{t_\mathrm{h}}{2}\mathcal{H}}, \tag{1}$$

$$A_u = A\left(1 - \frac{t_\mathrm{h}}{2}\mathcal{H}\right), \qquad A_l = A\left(1 + \frac{t_\mathrm{h}}{2}\mathcal{H}\right). \tag{2}$$

With this sign convention, monolayer configurations where polar head groups bend towards the bilayer's center (increasing monolayer's area compared to bilayer's midplane) have negative curvature and configurations bent in the opposite direction (with reduced area) have positive curvature. The number of lipids on each monolayer is denoted by $n_\alpha = n_{\alpha 1} + n_{\alpha 2}$, where $\alpha = u, l$ represents the monolayer and indexes 1 and 2 stand for the two lipid species. The local order parameter of a single monolayer is defined by $-1 \le \phi_\alpha = \frac{n_{\alpha 1} - n_{\alpha 2}}{n_\alpha} \le 1$.

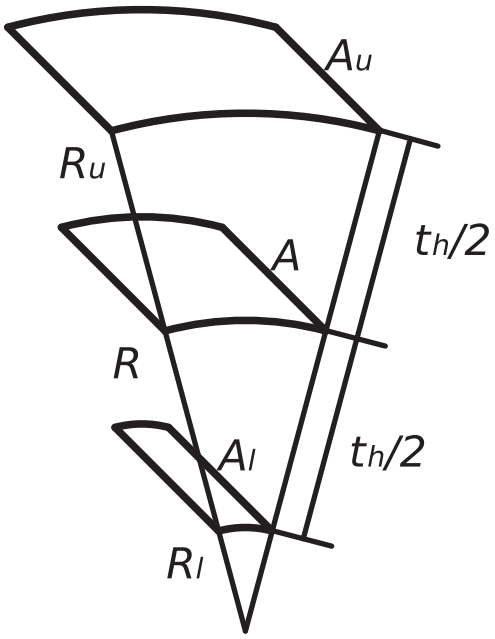

FIG. 1. Schematic representation of the curved bilayer, where the middle plane represents the neutral surface.

The free energy of the system can be decomposed into (i) the free-energy of mixing in the individual monolayer, (ii) a Helfrich Hamiltonian that describes the bending free energy of each monolayer, and (iii) a intrinsic coupling of the composition in the two apposing monolayers. In the following we study the composition of the monolayers at fixed curvature. Additionally, we neglect the intrinsic coupling (iii) of compositions between the two opposing monolayers due to interactions across the midplane of the membrane. Such phenomenological models have previously been studied.[3,12–18]

The free energy of mixing takes the form of an ideal mixture for each of the monolayers

$$\frac{F_\mathrm{mix}}{k_\mathrm{B}T} = \sum_{\{\alpha\}} n_\alpha \left[\frac{\chi}{4}(1-\phi_\alpha^2) + \frac{1+\phi_\alpha}{2}\ln\left(\frac{1+\phi_\alpha}{2}\right) + \frac{1-\phi_\alpha}{2}\ln\left(\frac{1-\phi_\alpha}{2}\right)\right], \tag{3}$$

where the first term quantifies the energy of mixing and the last two terms are the entropy of mixing. χ denotes the incompatibility due to pairwise repulsion of the species. This expression explicitly depends on the number of lipids per monolayer, n_α. For planar membranes $n_l \approx n_u$, however, for highly curved cylinders n_α must be proportional to the radius of the corresponding monolayer and, therefore, to its inverse curvature. To make this curvature dependence explicit we set $n_\alpha = \sigma_\mathrm{m} A_\alpha$, where A_α denotes the area of the corresponding monolayer and σ_m is the areal density of lipids in a monolayer, which may depend on membrane tension. The weak, quadratic dependence of σ_m on curvature is ignored.

We define the average order parameter, ψ, of the bilayer, which is linearly related to the average composition, and the composition difference, $\Delta\phi$, by

$$-1 \le \psi = \frac{\phi_l + \phi_u}{2} \le 1 \quad \text{and} \quad \Delta\phi = \frac{\phi_l - \phi_u}{2}. \tag{4}$$

Note that these definitions imply upper and lower limits for the values of $\Delta\phi$ that can be accessed for a fixed average composition. These saturation values are $\Delta\phi_\mathrm{s} = \pm(1 - |\psi|)$.

With these definitions for ψ and $\Delta\phi$, and according to Eqs. (1) and (2), the bilayer's free energy of mixing (up to first order in $\mathcal{H}$) takes the form

$$\frac{F_\mathrm{mix}}{\sigma_\mathrm{m} A k_\mathrm{B} T} = \mathrm{s}_l + \mathrm{s}_u + \frac{\chi}{2}(1 - \psi^2 - \Delta\phi^2) + \frac{h}{2}\mathcal{H}(\mathrm{s}_l - \mathrm{s}_u - \chi\psi\Delta\phi), \tag{5}$$

where we use the abbreviation

$$\mathrm{s}_\alpha = \frac{1+\phi_\alpha}{2}\ln\left[\frac{1+\phi_\alpha}{2}\right] + \frac{1-\phi_\alpha}{2}\ln\left[\frac{1-\phi_\alpha}{2}\right] \tag{6}$$

for the entropy of mixing of each planar monolayer. The second line in Eq. (5) is a correction to the free energy of mixing that accounts for the dilution or enhancement of interactions induced by curvature.

The free-energy cost of bending the bilayer membrane is described by a Helfrich Hamiltonian[23] for each of the

monolayers

$$\frac{F_{\rm ben}}{k_{\rm B}T} = \frac{\kappa_{\rm m}}{2} A_u (\mathcal{H}_u - C_u)^2 + \frac{\kappa_{\rm m}}{2} A_l (\mathcal{H}_l - C_l)^2, \quad (7)$$

where C_α is the spontaneous curvature of a single monolayer and $\kappa_{\rm m}$ denotes its bending rigidity, measured in units of the thermal energy scale, $k_{\rm B}T$. Since distinct lipid species are characterized by different spontaneous curvatures, C_α must be a function of the local order parameter. In the following, we assume a simple, linear dependence

$$C_\alpha = C_0 + \left(\frac{\sigma_{\rm m}}{\kappa_{\rm m}}\lambda\right)\phi_\alpha, \quad (8)$$

where C_0 is the spontaneous curvature of a mixed monolayer with an equal amount of lipids of each species, and λ quantifies the strength of the intrinsic curvature-composition coupling. The particular choice of the term in parenthesis recovers the usual definition for the coupling of the bilayer[15] (see last term in Eq. (11)). Alternatively, this definition provides an expression for λ and C_0 in terms of the spontaneous curvatures of the two lipid species, C_{+1} and C_{-1} (corresponding to $\phi_\alpha = \pm 1$)

$$\lambda = \frac{C_{+1} - C_{-1}}{2\eta_{\rm m}} \quad \text{and} \quad C_0 = \frac{C_{+1} + C_{-1}}{2}, \quad (9)$$

with $\eta_{\rm m} = \sigma_{\rm m}/\kappa_{\rm m}$. Typical values for the area per lipid and the bending rigidity at room temperature are $1/\sigma_{\rm m} \approx 0.5$ nm^2 and $\kappa_{\rm m} \approx 10.0$ (in units of $k_{\rm B}T$),[24,25] which yield the approximate value $\eta_{\rm m} \approx 0.2$ nm^{-2}. Additionally, the absolute spontaneous curvature of lipids with biological relevance has been reported[25] to be as large as $|C_{\pm 1}| \approx 0.9$ nm^{-1}. These data provide us with a crude estimate for the absolute value of the strength of the direct coupling, $|\lambda| \lesssim 4.5$ nm.

Expanding the bending energy of the bilayer, Eq. (7), up to first-order terms in $\mathcal{H}$, we obtain

$$\frac{F_{\rm ben}}{\sigma_{\rm m} A k_{\rm B} T} = t_{\rm h}\mathcal{H}\Delta\phi[C_0\lambda + \eta_{\rm m}\lambda^2\psi] + 2\lambda\mathcal{H}\Delta\phi + \eta_{\rm m}\lambda^2\Delta\phi^2 + \text{terms independent from } \mathcal{H} \text{ and } \Delta\phi. \quad (10)$$

The last term in this expression can be absorbed into the definition of the bare χ parameter in Eq. (5). We define the effective incompatibility coefficient $\chi_{\rm eff} = \chi - 2\eta_{\rm m}\lambda^2$.

Adding the mixing and bending contributions, Eqs. (5) and (10), we obtain the final expression for the free energy of the bilayer:

$$\frac{F}{\sigma_{\rm m} A k_{\rm B} T} = {\rm s}_l + {\rm s}_u + \frac{\chi_{\rm eff}}{2}(1 - \psi^2 - \Delta\phi^2) + \frac{t_{\rm h}}{2}\mathcal{H}({\rm s}_l - {\rm s}_u - \chi_{\rm eff}\psi\Delta\phi) + t_{\rm h}\mathcal{H}\Delta\phi(C_0\lambda + \eta_{\rm m}\lambda^2\psi) + 2\lambda\mathcal{H}\Delta\phi. \quad (11)$$

The most probable composition difference, $\Delta\phi^*$, for a fixed average order parameter, ψ, and curvature, $\mathcal{H}$, is obtained by minimizing Eq. (11)

$$0 = \frac{1}{2}\ln\left[\frac{(1+\Delta\phi^*)^2 - \psi^2}{(1-\Delta\phi^*)^2 - \psi^2}\right] + \frac{t_{\rm h}\mathcal{H}}{4}\ln\left[\frac{(1+\psi)^2 - \Delta\phi^{*2}}{(1-\psi)^2 - \Delta\phi^{*2}}\right] - \chi_{\rm eff}\Delta\phi^* - \frac{1}{2}\chi_{\rm eff} t_{\rm h}\mathcal{H}\psi + t_{\rm h}\mathcal{H}\left(C_0\lambda + \eta_{\rm m}\lambda^2\psi\right) + 2\lambda\mathcal{H}. \quad (12)$$

If the composition difference between monolayers is small, compared to the corresponding saturation value for the given average order parameter, $|\Delta\phi^*| \ll |\Delta\phi_{\rm s}|$, this equation can be further approximated by

$$-\left[\frac{2}{1-\psi^2} - \chi_{\rm eff}\right]\Delta\phi^* = t_{\rm h}\mathcal{H}\left[\frac{1}{2}\ln\left(\frac{1+\psi}{1-\psi}\right) - \frac{1}{2}\chi_{\rm eff}\psi\right] + \lambda t_{\rm h}\mathcal{H}\left[\frac{2}{t_{\rm h}} + C_0 + \eta_{\rm m}\lambda\psi\right], \quad (13)$$

which predicts a linear dependence of the most probable composition difference, $\Delta\phi^*$, on curvature. The strength of this dependence is given by the effective curvature-composition coupling

$$\frac{\Lambda_{\rm eff}}{t_{\rm h}} = \frac{\frac{1}{2}\ln\left[\frac{1+\psi}{1-\psi}\right] + \psi[\eta_{\rm m}\lambda^2 - \frac{1}{2}\chi_{\rm eff}] + \lambda[\frac{2}{t_{\rm h}} + C_0]}{\chi_{\rm eff} - \frac{2}{1-\psi^2}}. \quad (14)$$

Phase separation in the monolayers of a planar membrane will occur, if $\chi_{\rm eff}$ exceeds the critical value χ_c. The mean-field estimate for the critical point is $\chi_c^{\rm MF} = 2$. If the planar membrane does not spontaneously phase separate (i.e., $\chi_{\rm eff} < 2$), the bracket on the left-hand side of Eq. (13), which quantifies the inverse susceptibility of the bilayer with respect to composition fluctuations, will be positive.

Note that $\Lambda_{\rm eff}$ is not an odd function of the average order parameter ψ, i.e., it does not simply change sign when the two lipid species are exchanged. The last term in the numerator of Eq. (14) quantifies this asymmetry and it is proportional to the intrinsic coupling, λ, and the sum of the curvature of a single, mixed monolayer and its maximum attainable value, $2/t_{\rm h}$. (The maximum radius of curvature of a monolayer is $t_h/2$, as can be seen in Fig. 1).

If the susceptibility is large, i.e., in the proximity of macroscopic demixing of the planar membrane, this curvature-induced asymmetry will be enhanced and the complementary distribution of lipids between monolayers (opposite composition in opposite leaflets, as described in Ref. 26) will be more pronounced. This requirement of co-operativity is also supported by experiments on curvature-induced lipid sorting.[27]

III. MODELS AND SIMULATION TECHNIQUE

In order to study the curvature-composition coupling in mixed bilayer membranes, we employ a minimal, implicit-solvent model,[19–21] and the coarse-grained MARTINI model.[22] The former model serves to systematically

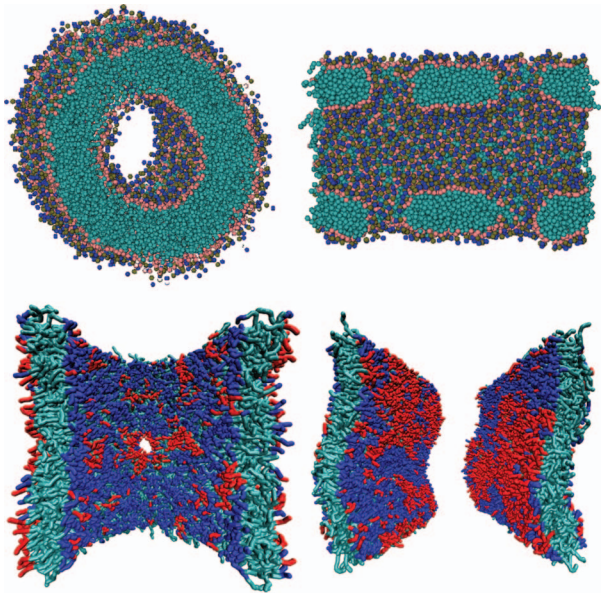

FIG. 2. Snapshots of configurations used in this work. (Top left) A configuration for the cylindrical geometry of the MARTINI model. (Top right) Cut of the same configuration along the cylinder axis. The 4 pores opened in the membrane to allow a fast exchange of lipids between inner and outer leaflets are clearly observed. (Bottom left) Axial cut of a cylinder used in the implicit-solvent model. The white spot in the middle is the pore used to facilitate the equilibration of areal densities in both leaflets. (Bottom right) Upper and lower views of a planar configuration used in the implicit-solvent simulations.

explore the effects of curvature-composition coupling and to compare the results of planar membranes with thermal fluctuations of the local bilayer position and highly curved membrane tubes. The latter model allows us to make direct connection to relevant experimental systems. Snapshots of typical configurations used in both, MARTINI and implicit-solvent simulations are shown in Fig. 2.

Details of model parameters and setup of simulations are compiled in Appendix A.

IV. RESULTS

A. Minimal, implicit-solvent membrane model

First, we characterize the dependence of the order parameter, ψ, for nearly planar membranes, as function of the imposed exchange chemical potential, $\Delta\mu$. As shown in Fig. 3, the transition from the regime where the bilayer is mainly composed of short-head lipids to the one where the majority component are large-head lipids, occurs in a narrower interval for the high incompatibility case than in the case of small incompatibility. Therefore, composition fluctuations are stronger in the former case and the effective curvature-composition coupling is expected to be enhanced. The susceptibility of the order parameter, S_ψ, was extracted from the slope of the graphs in the main plot of Fig. 3. Consistent results were obtained from the analysis of fluctuations of ψ,[28,29] as shown in the inset of Fig. 3, for the case of low incompatibility. This susceptibility is related to the second

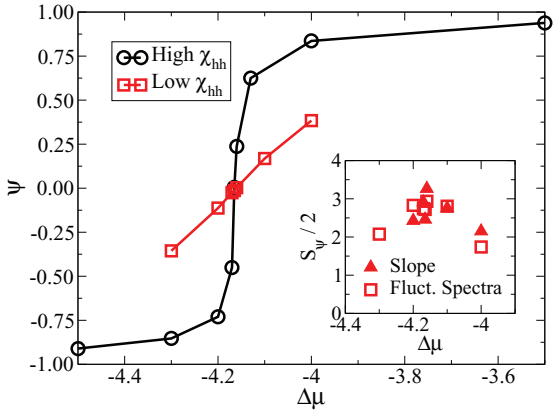

FIG. 3. Main plot: Average order parameter, ψ, of the minimal, implicit-solvent model vs exchange chemical potential, $\Delta\mu$, for low and high incompatibilities (lines are just guides to the eye). Inset: Susceptibility of local composition for low incompatibility, evaluated from the slope of the corresponding graph in the main plot (filled triangles) and the analysis of composition fluctuations (open squares).

derivative of the free energy, Eq. (11), via

$$\left[\frac{\partial\langle\psi\rangle}{\partial\Delta\mu}\right]^{-1} = \frac{1}{\sigma_m A\langle(\psi-\langle\psi\rangle)^2\rangle} \equiv \frac{2}{S_\psi} = \frac{1}{\sigma_m A}\frac{\partial^2 F/k_B T}{\partial\psi^2} = -\chi_{\text{eff}} + \frac{2}{1-\psi^2}. \quad (15)$$

From this analysis we found $\chi_{\text{eff}}^L = 1.5 \pm 0.3$ and $\chi_{\text{eff}}^H = 1.97 \pm 0.1$, for low and high incompatibility, respectively.

After composition fluctuations are equilibrated around an average value set by $\Delta\mu$, we map the unit length of our simulations, i.e., the cutoff radius for non-bonded interactions, r_c, to real units. This is done by means of the bilayer thickness, which we defined as the distance between peaks in the density profile, for head-group beads in opposite leaflets, finding $t_h \approx 6r_c$. Since the typical thickness of real biological membranes is in the range of several nanometers, we can identify $r_c \approx 1$ nm. Once this is done, we can analyze the local shape and composition of the bilayer using a lateral grid of 8×8 squares in the xy plane. Then, at every grid point, we fit the height of the membrane (with respect to its projected plane) by a quartic function

$$g(x, y) = p_1x^2 + p_2y^2 + p_3xy + p_4x + p_5y + p_6. \quad (16)$$

In this Monge representation, the mean curvature $\mathcal{H}$ is given by[30]

$$\mathcal{H} = \frac{(1+g_y^2)g_{xx} - 2g_xg_yg_{xy} + (1+g_x^2)g_{yy}}{2(1+g_x^2+g_y^2)^{3/2}}, \quad (17)$$

and the derivatives are locally estimated from a fit according to Eq. (16). In the limit of small curvatures, we consider only first-order terms, so that this expression simplifies to

$$\mathcal{H} = \frac{g_{xx}+g_{yy}}{2}, \quad (18)$$

i.e., the mean curvature at a given point, (x, y), on the membrane is computed from the fit according to $\mathcal{H} = p_1 + p_2$.

The fit is done using the sub-grid with 4×4 neighbors of the current point. The concentration difference at that point

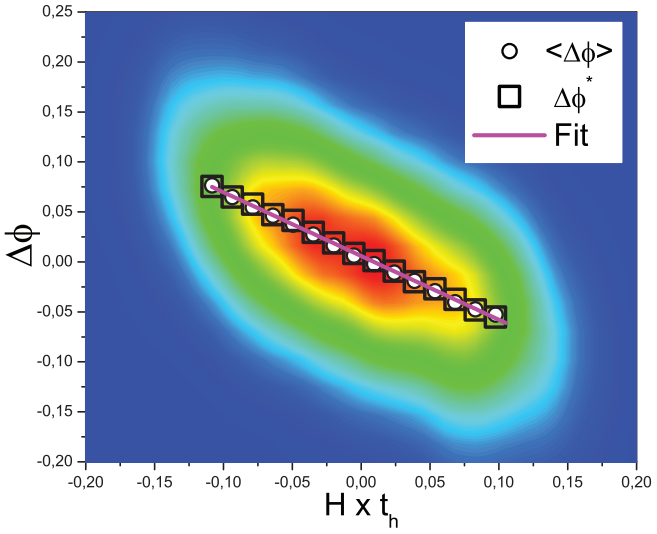

FIG. 4. Color map: Joint probability distribution of local curvature, $\mathcal{H}$, and composition difference, $\Delta\phi$, for $\Delta\mu = -4.130$. Symbols: Average $\langle\Delta\phi\rangle$ and most probable, $\Delta\phi^*$ composition difference for a given curvature. The line is a linear fit, $\Delta\phi^*$ vs. $t_h\mathcal{H}$, from which we determine the effective composition-curvature coupling, Λ_{eff}.

is set as the average concentration difference on the same sub-grid. A typical snapshot of a membrane with pronounced shape and composition fluctuations is shown in Fig. 2. This snapshot also exhibits the high degree of complementarity between the two leaflets (opposite composition on opposite leaflets) for systems close to the demixing critical point (i.e., for high incompatibility and $\Delta\mu \approx -4.160$, shown in Fig. 3).

From those maps we evaluate the joint-probability distribution function, $P(\mathcal{H}, \Delta\phi)$, counting all the occurrences of a particular $\Delta\phi$ for a given $\mathcal{H}$. Fig. 4 presents $P(\mathcal{H}, \Delta\phi)$ for the case $\Delta\mu = -4.130$.

From every histogram (one per each $\Delta\mu$) we obtained the most likely, $\Delta\phi^*$ and the average, $\langle\Delta\phi\rangle$ composition difference for a given curvature. Away from the critical point of demixing, $\Delta\phi$ is Gaussian distributed and both values coincide. However, near the critical point, finite-size effects become important and the distribution slightly deviates from a Gaussian, as shown in Fig. 5 for the composition difference, $\Delta\phi$, and the reduced order-parameter, $\frac{\psi-\langle\psi\rangle}{\sigma}$ (with $\langle\psi\rangle$ and σ being the mean and standard deviation of the distribution, respectively). This non-Gaussian behavior is a characteristic feature of critical phenomena.[31–35] In those cases, we have considered the most probable composition difference, $\Delta\phi^*$, for the analysis (cf. inset in Fig. 5).

The coefficient $\eta_m = \sigma_m/\kappa_m$ in the definition of the effective coupling, Eq. (14), was determined by measuring (i) the surface density of lipids in each monolayer and (ii) the fluctuation spectra of the bilayer in the limit of small wave vectors ($\lim_{q\to 0} S(q) = \frac{1}{A\kappa_m q^4}$), from which the bending rigidity, κ_m, was obtained. No significant differences where found for low and high incompatibility, or data corresponding to different average compositions. We set the average value $\eta_m = 0.1685 \pm 0.0033\ \text{nm}^{-2}$, which corresponds to $\kappa_m \approx 10.6$. This result lies within typical values reported for single component, fluid phase membranes.[19]

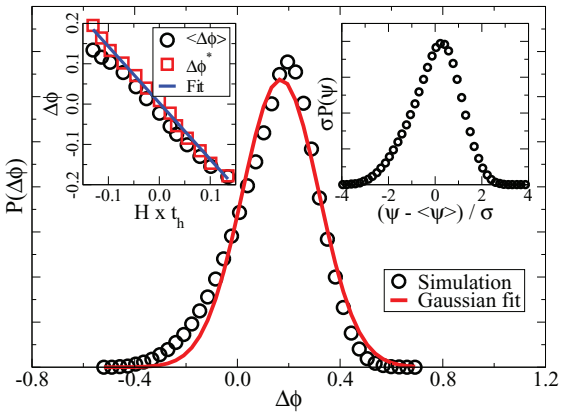

FIG. 5. Main plot: Probability distribution function for composition difference, $\Delta\phi$, slightly above the critical point, $\Delta\mu = -4.160$ and high incompatibility. Insets: (Left) Average, $\langle\Delta\phi\rangle$, most probable, $\Delta\phi_{\text{max}}$ and fitted composition difference for a given curvature. (Right) Probability distribution of the reduced order parameter, $\frac{\psi-\langle\psi\rangle}{\sigma}$.

Analyzing the joint probability distribution, cf. Fig. 4, we determine the effective coupling, Λ_{eff}. The results as a function of the average order parameter, ψ, and two incompatibilities are presented in Fig. 6. Globally fitting these simulation results to the prediction of the phenomenological theory, Eq. (13), we obtained the parameters, C_0, λ, and χ for low and high incompatibility cases. A compilation of relevant parameters for the implicit-solvent model is given in Table I. Using this simple set of parameters, we can describe the effective coupling, Λ_{eff}, for different average compositions and incompatibilities, indicating that the phenomenological description captures the salient physical mechanisms of composition-curvature coupling for our membrane model.

Several conclusions can be drawn from these results:

- $C_0 = -0.27\ \text{nm}^{-1} \leq 0$. This, together with Eq. (8) yields $C_{+1} = 0.072\ \text{nm}^{-1}$ and $C_{-1} = -0.61\ \text{nm}^{-1}$ for the spontaneous curvatures of the short-head and large-head lipids, respectively. Additionally, these results are consistent with those presented in Ref. 19, where short-head lipids are reported to self assembly into planar bilayers, whereas large-head ones are close to the phase boundary between planar bilayers and cylindrical micelles.

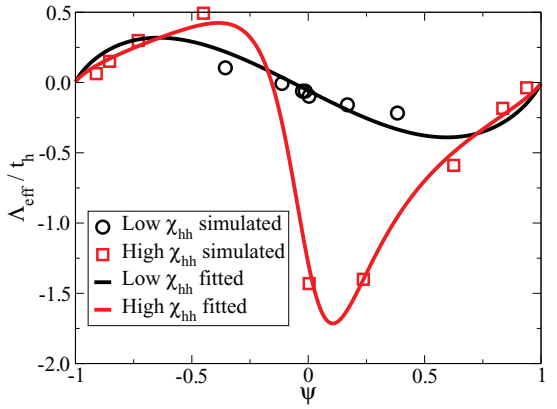

FIG. 6. Effective coupling vs average order parameter for low and high incompatibility.

TABLE I. Phenomenological parameters for simulations with the minimal, implicit-solvent model.

Param.	Value	Param.	Value
t_h	6.0 nm	η_m	$0.1685 \pm 0.0033\ \text{nm}^{-2}$
κ_m	10.6 ± 0.3	C_0	$-0.27 \pm 0.01\ \text{nm}^{-1}$
λ	2.01 ± 0.06 nm	χ_{eff}^L	0.0 ± 1.13
χ_{eff}^H	1.91 ± 0.01		

- $\lambda \geq 0$ reflects the fact that lipids with shorter/larger head groups will prefer to cluster in regions with positive/negative curvature, respectively.
- The agreement over the entire range of compositions validates the linear dependence of the spontaneous curvature of a mixed monolayer on composition, Eq. (8).
- $\chi_{\text{eff}} = 1.91 \lesssim \chi_c$ for high incompatibility. In this case, the system is fairly close to the critical point of macroscopic phase separation. This result is in agreement with the finite-size effects and the non-Gaussian probability distribution function of $\Delta\phi$ near $\Delta\mu \approx -4.160$ (cf. Fig. 5), where the correlation length is comparable to the system size. It is also in good accord with the analysis of Fig. 3 and Eq. (15). Recent experimental observations suggesting that the composition of plasma membranes is tuned close to a miscibility critical point[36] indicate the relevance of near-critical conditions.
- $\chi_{\text{eff}} \approx 0$ for low incompatibility. Qualitatively, the incompatibility is lower than for the high incompatibility case but, quantitatively, the estimate extracted from Fig. 6 is smaller than the value obtained from Fig. 3. This deviation can be partially rationalized by the insensitivity of the data in Fig. 6 to the value of χ_{eff}, that is reflected in the rather large uncertainty of the fit. Moreover, an additional term in the free energy of mixing that stems from the coupling of the composition of the two opposing monolayers, could become important at small incompatibility but such a term has been neglected in our phenomenological treatment. Finally, also the composition-dependence of the mechanical properties of the bilayer could generate additional terms that help explain the deviation at low incompatibility.
- It is also worth noting that the values of λ, C_0, and η_m are in good agreement with what is expected for biologically relevant lipids, according to the analysis following Eq. (9).

From Fig. 6 we also observe that the model reproduces the expected behavior for single-component systems (those with $\psi = \pm 1$), where the effective coupling vanishes, since the compositions difference remains zero, no matter what the curvature of the bilayer is.

Another feature is the predicted asymmetry with respect to equi-molar composition, $\psi = 0$. As previously discussed, this effect is enhanced when the system is in the vicinity of the demixing critical point, where the intrinsic coupling and the enthalpic contributions become comparable to the entropic term, which tends to smooth out composition heterogeneities.

The phenomenological expression for the effective coupling, Eq. (14), has been obtained in the limit that the composition difference is small compared to its saturation value, $\Delta\phi_s$. The validity of this assumption depends on the strength of the effective coupling. In particular, high curvatures as they occur in membrane tethers and high incompatibility will results in the break-down of the linear dependence. Instead, those systems will be described by the implicit relation Eq. (11), which duly accounts for saturation effects that stem from the free energy of mixing. This hypothesis is verified by simulations with highly curved cylinders of different radii at both, high and low, incompatibility. For these simulations, the total number of lipids in each leaflet has been equilibrated by opening a small pore oriented in the direction perpendicular to the axis of the cylinder, as described in Appendix A 2 (see Fig. 2). The results are shown in Fig. 7, where continuum and broken lines correspond to the numerical solution of Eq. (11) using the parameters of the phenomenological model extracted from Fig. 6, squares represent data from simulations with planar membranes and circles correspond to simulations with narrow cylinders. The saturation values for low and high incompatibility are $\Delta\phi_s = 0.62$ and $\Delta\phi_s = 0.763$, respectively. In all cases we observe good agreement between simulations and phenomenological description. For planar cases, we corroborate that the linear approximation accurately described the range of curvatures accessible to flat bilayers. Moreover, due to the small effective coupling, the linear approximation remains valid for cylinders with low incompatibility. Only for narrow cylinders with high incompatibility, we observe that corrections due to the entropy of mixing become important and the full description, Eq. (11), nicely agrees with our simulation data in the limit $\Delta\phi \to \Delta\phi_s$.

B. MARTINI coarse-grained model

For the MARTINI model we simulated binary 1:1 mixtures, corresponding to $\psi = 0$, comprised of a cylinder-shaped lipid, dipalmitoylphosphatidylcholine (DPPC), as a common component in all of them. The second species, phosphatidylethanolamine, was a conically shaped lipid with a PE head group. PE is a major lipid of the plasma membrane, representing about 25% of the phospholipids, with an

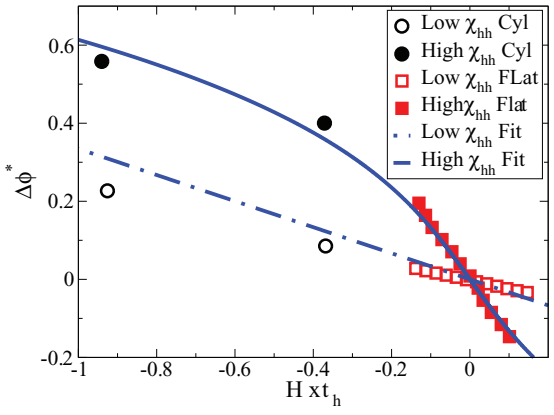

FIG. 7. Most probable composition difference *vs* curvature for high and low incompatibility.

asymmetric distribution between the leaflets.[37] Upon dehydration and/or temperature increase, PE lipids tend to form inverted hexagonal (H_{II}) phases.[38–40] Tails of PE were changed in the number and type of unsaturations to account for the effect of the tail region on the curvature preference of the lipid. We took DPPE which has fully saturated tails of the same kind as those in DPPC; POPE and DOPE with one or both monounsaturated tails, respectively; PUPE and DUPE, having one or both polyunsaturated tails, respectively. The unsaturated species of PE are the more prevalent ones in natural membranes. Within the MARTINI model, the difference between PE and PC represents the ability of PE to form hydrogen-bonds between neighbor PE molecules.

To quantify $\eta_{\rm m} = \frac{\sigma_{\rm m}}{\kappa_{\rm m}}$, we determined the areal density and the bending rigidity of the bilayers. $\kappa = 2\kappa_m$ was measured in the cylindrical geometry as proposed in Ref. 41

$$\kappa = \frac{F_z R}{2\pi}, \tag{19}$$

where F_z is the force needed to keep the cylinder length constant and R denotes the cylinder radius (see Fig. 1). The net force along the z-direction is computed according to

$$F_z = \left(P_{zz} - \frac{P_{xx} + P_{yy}}{2} \right) L_x L_y, \tag{20}$$

where P_{ii} are the pressure components along the x, y, and z axis and $L_x L_y$ is the box area perpendicular to the cylinder. We also obtained κ from the fluctuation spectra of planar membranes at $q \to 0$. Both values are given in Table II. We observe a slight decrease of the bending rigidity with the radius in accord with previous simulations of the MARTINI model.[42] This curvature dependence of the mechanical properties results from the modification of the lipid packing upon bending. In mixtures DOPE-DPPC the smaller cylinder is about 1.5 times more rigid, but the largest cylinder simulated shows almost no differences with a planar bilayer. The areal density, $\sigma_{\rm m}$, and membrane thickness, $t_{\rm h}$, also exhibit a weak curvature dependence. For $R \approx 7$ nm, however, both values are within 2% of those of the planar geometry.

The incompatibility between the lipid species was estimated from the susceptibility of the local composition, ψ, in

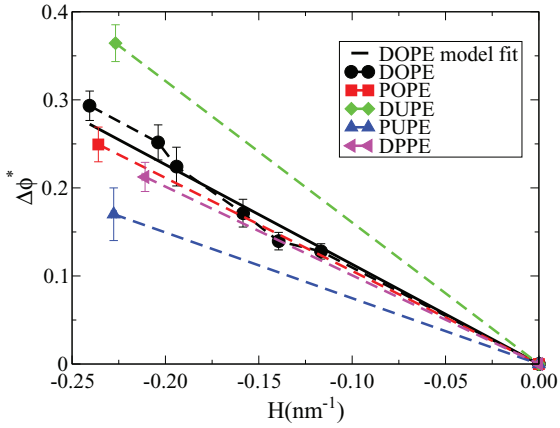

FIG. 8. Composition, ϕ, as a function of curvature, $\mathcal{H}$, for 1:1 binary mixtures of DPPC and a PE (see Legend), in cylindrical bilayers at $T = 300$ K. Dashed lines are guides to the eyes. Thick line is the fit of Eq. (13) for the average value of parameters reported in Table II for the DOPE series.

NpT or NVT ensembles with fixed total composition, as described in Sec. IV A, Eq. (15). To this end, we divided a planar patch of membrane into a square grid of about $\Delta L = 5$ nm length. Each grid cell is comprised of about 40 lipids and the composition is equi-molar on average, $\langle \psi \rangle = 0$. Thus, the incompatibility is estimated according to $\chi_{\rm eff} = 2 - 2/S_\psi$.

The effective composition-curvature coupling, $\Lambda_{\rm eff}$, was estimated from the linear dependence of the composition difference, $\Delta\phi$, on the curvature, $\mathcal{H}$, of a cylindrical membrane tube as shown in Fig. 8. The error bars are the standard deviation of the data. We chose the mixture DPPC-DOPE to make a systematic variation of cylinder radius in the range 4 nm to 9 nm. Although these radii are well below the typical radii of experiments, $R \approx 25$ nm,[44] the simulations of the more-detailed MARTINI model are already computationally intense. Even larger radii would increase the system size and reduce the composition difference, $\Delta\phi$, and thereby make the study unfeasible with the computational resources available to us. The simulations of the implicit-solvent model, which allows us to study small and large curvatures, however, suggest (cf. Fig. 7) that the values extracted from highly curved cylinders are also indicative of the behavior of larger tubes or planar membranes.

TABLE II. Membrane properties of MARTINI bilayers made of 1:1 mixtures of DPPC and the lipid listed in the first column. The spontaneous curvature of DPPC lipids, $C_{\rm PC} = 0.035$ nm^{-1}, was extracted from literature.[43] The radius of the membrane tube was varied for mixtures DPPC-DOPE: Radius, R, thickness, $t_{\rm h}$, areal density, $\sigma_{\rm m}$, bilayer bending constant measured in the cylinders using Eq. (19), κ, and in planar membranes from the fluctuation spectra, κ^*; effective incompatibility coefficient, $\chi_{\rm eff}$, direct curvature-composition coupling, λ and spontaneous curvature for $C_{\rm PE}$ lipid species (check sign convention defined in Sec. II).

System	R (nm)	t_h (nm)	$\sigma_{\rm m}$ (nm^{-2})	κ ($k_{\rm B}T$)	κ^* ($k_{\rm B}T$)	$\Lambda_{\rm eff}$ (nm)	$\chi_{\rm eff}$	λ (nm)	$C_{\rm PE}$ (nm^{-1})
DOPE_4	4.16 ± 0.02	4.30 ± 0.03	1.455 ± 0.008	28.8 ± 0.4	20.0 ± 0.9	-1.22 ± 0.07	-0.19 ± 0.07	1.03 ± 0.04	0.24 ± 0.01
DOPE_4.9	4.90 ± 0.02	4.35 ± 0.04	1.553 ± 0.008	25.2 ± 0.5		-1.23 ± 0.10		1.00 ± 0.05	0.28 ± 0.01
DOPE_5	5.15 ± 0.03	4.39 ± 0.04	1.538 ± 0.009	23.7 ± 0.5		-1.16 ± 0.11		0.94 ± 0.05	0.28 ± 0.01
DOPE_6	6.31 ± 0.04	4.41 ± 0.06	1.567 ± 0.01	22.7 ± 0.7		-1.08 ± 0.10		0.88 ± 0.07	0.28 ± 0.02
DOPE_7	7.17 ± 0.03	4.40 ± 0.05	1.582 ± 0.008	21.4 ± 0.9		-1.00 ± 0.07		0.81 ± 0.09	0.28 ± 0.02
DOPE_9	8.57 ± 0.04	4.40 ± 0.06	1.594 ± 0.008	18.7 ± 2		-1.10 ± 0.07		0.86 ± 0.20	0.32 ± 0.06
POPE	4.24 ± 0.04	4.21 ± 0.06	1.54 ± 0.02	30.8 ± 0.9	24.8 ± 0.5	-1.06 ± 0.08	-0.20 ± 0.04	0.92 ± 0.09	0.22 ± 0.02
DUPE	4.41 ± 0.03	3.84 ± 0.04	1.46 ± 0.01	15.6 ± 0.5	14.1 ± 0.4	-1.61 ± 0.09	1.38 ± 0.01	0.41 ± 0.05	0.19 ± 0.02
PUPE	4.39 ± 0.02	3.94 ± 0.04	1.503 ± 0.009	21.0 ± 0.5	18.8 ± 0.4	-0.75 ± 0.13	0.25 ± 0.05	0.53 ± 0.05	0.19 ± 0.01
DPPE	4.74 ± 0.04	4.17 ± 0.05	1.63 ± 0.01	32.4 ± 0.7	23.2 ± 0.3	-1.00 ± 0.08	-0.22 ± 0.03	0.89 ± 0.07	0.21 ± 0.01

Fig. 8 indicates that in mixtures DOPC-DOPE the linear dependence of the composition difference, $\Delta\phi$, on the curvature, $\mathcal{H}$, is approximately obeyed. The small deviations from the linear behavior can be partially traced back to the curvature-dependence of the bending rigidity (cf. Appendix B).

Using the phenomenological model in Sec. II and the independently determined values of $\eta_{\rm m}$ and $\chi_{\rm eff}$, we calculated the spontaneous curvature, C_0, of a mixed monolayer and the intrinsic composition-curvature coupling, λ, for the different bilayers. For equi-molar mixtures, $\psi = 0$, Eq. (14) simplifies to

$$\Lambda_{\rm eff} \equiv \frac{\Delta\phi^*}{\mathcal{H}} = -\frac{\lambda(2 + C_0 t_{\rm h})}{2 - \chi_{\rm eff}}. \tag{21}$$

Using the relation between the spontaneous curvatures for one-component monolayers and the parameters, C_0 and λ, cf. Eq. (8), we obtain

$$\Lambda_{\rm eff} = \frac{(C_{\rm PE} - C_{\rm PC})[4 + t_{\rm h}(C_{\rm PE} + C_{\rm PC})]}{4\eta_{\rm m}(2 - \chi_{\rm eff})}, \tag{22}$$

where $C_{\rm PC} = C_{-1}$ stands for the spontaneous curvature of PC and $C_{\rm PE} = C_{+1}$ for that of PE. In the following, we use the pure DPPC membrane as a reference system and assume the independently measured spontaneous curvature, $C_{\rm PC} = 0.035\ {\rm nm}^{-1}$, extracted from the bilayer stress profile in Ref. 43. Equation (22) then yields the spontaneous curvatures for all the mixing partner. The results for $C_{\rm PE}$ and λ are presented in Table II. First, the trend in spontaneous curvatures is as expected, with higher positive values for the inverted conically shaped PE lipids compared to PC lipids, as evidenced by a positive λ. The equi-molar mixtures have positive spontaneous curvatures, C_0, meaning that monolayers curve towards the hydrophilic region. Values of $C_{\rm PE}$ for DOPE and DPPE are well in agreement with those reported for these lipids within the MARTINI model from pressure profile measurements.[22,43] The spontaneous curvatures of the modeled lipids are, however, slightly underestimated in comparison with the available experimental data on DOPE and POPE. $C_{\rm DOPE}$ values from literature range from $0.33\ {\rm nm}^{-1}$ to $0.39\ {\rm nm}^{-1}$,[45–47] and $C_{POPE} = 0.29\ {\rm nm}^{-1}$ has been reported in Ref. 47. The difference between POPE and DOPE is quite well reproduced within the MARTINI model.

Comparing lipids with identical hydrocarbon tails (i.e., DPPC and DPPE), there is a 6 times increase in the spontaneous curvature. Thus, the head group likely is the major contribution to the increase in spontaneous curvature from PC lipids to PE lipids.

The effect of changes in the hydrocarbon region on C_{PE} is significantly smaller. The increase in the hydrophobic volume would putatively result in a larger curvature.[48,49] PE lipids with monounsaturated tails (i.e., POPE and DOPE) follow this rationale: They show enhanced preference for positively curved regions, but the increase in spontaneous curvature is only about 30% with respect to the saturated PE(DPPE).

Polyunsaturated tails (i.e., PUPE and DUPE), however, are characterized by spontaneous curvatures similar to DPPE, despite the lower packing density and larger hydrocarbon volume.[50,51] This agrees with previous results that show that the high rate of back-bending in the tails may help polyunsaturated PC lipids to adapt to negative (convex) curvatures by providing the hydrocarbon tail region with a wedge shape.[52] In line with our data, changes in the transition temperature from the lamellar (L_α) to the inverted hexagonal (H_{II}) phase was shown to be rather insensitive to different hydrocarbon chain structures in PE lipids.[49]

Undersaturation of the tails also affects the effective composition-curvature coupling, $\Lambda_{\rm eff}$, via the increase of the incompatibility. In fact, the mixture DPPC-DUPE is characterized by the largest effective composition-curvature coupling. The data in Table II show that $\chi_{\rm eff}$ is larger for mixtures of DPPC with a polyunsaturated PE lipids (i.e., PUPE and DUPE) than monounsaturated PE lipids (i.e., POPE and DOPE). This demixing tendency, and thereby the effective composition-curvature coupling, can be further enhanced by the addition of cholesterol.[53–55]

Comparing the results of the minimal, implicit-solvent model and the coarse-grained MARTINI model we observe that (i) the two lipid species have different spontaneous curvatures in the implicit-solvent model whereas they have both positive spontaneous curvatures in the MARTINI model and (ii) the difference in spontaneous curvatures and the composition-curvature coupling is larger in the implicit-solvent model than in the MARTINI model because the pair of lipids in the MARTINI are more similar than those in the implicit-solvent model. In the MARTINI model, both head groups, PE and PC, are comprised of two particles. The one, representing the phosphate group, is the same for both type of molecules. The other, representing the amine region, differs in order to allow for stronger headgroup-headgroup interactions in PE lipids.[56] In the implicit-solvent model, however, the lipid species differ in their hydrophilic-hydrophobic asymmetry that is directly related to the spontaneous curvature of a monolayer. The strong dependence of the spontaneous curvature on the fraction, f, of hydrophobic beads has also been observed in studies using similar models,[57,58] where the change of a hydrophilic to a hydrophobic bead drastically changes the excess free energy of forming an hourglass-shaped passage ("stalk") between apposing membranes. These passage become metastable in the vicinity of the transition between the L_α and the H_{II} phase. Previous studies indicate that stalks become metastable around $f \approx 0.9$,[57] i.e., the value $f = 0.6875$ and $f = 0.75$ correspond to rather cone-shaped lipids.

V. SUMMARY AND OUTLOOK

In this work we have presented a phenomenological model to describe the effective coupling between curvature and composition in a two-component lipid bilayer. In addition to the elastic energy of the membrane and an intrinsic coupling between curvature and composition, our model also includes contributions from a composition- and curvature-dependent free energy of mixing. Low incompatibility between different lipid species leads to a weak effective composition-curvature coupling because the elastic energy gain due to lateral lipid sorting into regions of favored curvature cannot overcome the concomitant entropy loss. High incompatibility, however, results in much larger effects

where in addition to the intrinsic coupling, the curvature dependence of the free energy of mixing contributes to the lateral sorting of lipids. This combined effect results in a higher coupling that is further enhanced as the system approaches the demixing critical point.

The quantitative comparison between the phenomenological model and computer simulation of a coarse-grained, implicit-solvent membrane model demonstrates that a single set of parameters can consistently describe the behavior for different average compositions of the mixed membrane and different incompatibilities. Additionally, we have obtained consistent results comparing planar membranes where thermal fluctuations induce small curvature fluctuations and highly curved membrane tubes that are characterized by strong, average curvatures.

Applying this validated model of composition-curvature coupling, we have investigated the composition-curvature coupling in mixed membrane tubes and the spontaneous curvature of monolayers within the MARTINI model.[22] Varying the head group architecture and the saturation of hydrophobic tails, we have obtained the spontaneous curvatures of a variety of biologically relevant lipids.

Our computational strategy offers an alternative to obtaining the spontaneous curvature from moments of the stress profile across a bilayer membrane.[11] Since the measurement of bending rigidity[41] and composition-curvature coupling can be efficiently performed in the highly curved geometry of a membrane tube we expect that this strategy will find further application. Whereas membrane properties in minimal coarse-grained models are rather insensitive to curvature,[41] models that account for more details of the lipid packing may exhibit a dependence of the membrane properties on curvature (see, e.g., Table II). Our results indicate that such a dependence is smaller for the composition-curvature coupling than for the bending rigidity, but such a dependence can be accounted for by the phenomenological model (see Appendix B).

ACKNOWLEDGMENTS

It is a great pleasure to thank S. Sadeghi, M. Schick, and R. L. C. Vink for stimulating discussions and H. J. Risselada and Y. Smirnova for sharing with us the implementation of the pore formation. Financial support by the German Science Foundation within the SFB 937 "Collective behavior of soft and biological matter" TP A7, the German Academic Exchange Service (DAAD), the National Council of Science and Technology (CONACyT), as well as CONICET (PIP 112-200801-00403), MINCYT (11/09, PICT-2011-1887), and INN-CNEA (2011) grants are gratefully acknowledged. Computing in the HLRN Hannover/Berlin and the JSC Jülich, Germany is also gratefully acknowledged.

APPENDIX A: MODELS AND SIMULATION TECHNIQUE

1. Minimal, implicit-solvent membrane model

We consider the bilayer as a binary mixture of lipids differing in their head group only. In this way, the formation of local inhomogeneities will be driven mainly by interactions within a single monolayer, i.e., the coupling of composition fluctuations across a planar membrane is small. In this case, we expect the curvature-composition coupling to result in complementary arrangement of domains in the two apposing leaflets.

In our minimal, implicit-solvent model,[19–21] n lipids are represented by linear chains consisting of $N = 16$ segments. The number of segments of the head group is N_α and this value differs between the two lipid species. The first lipid species is comprised of $N_B = 4$, B-type head beads and $N_A = N - N_B = 12$ hydrophobic tail beads of type A. The second lipid species is characterized by 5 head beads of segment type C and 11 tail beads of segment type A. The different ratios of hydrophilic and hydrophobic portions gives rise to differences in the spontaneous curvature.

The architecture of the flexible amphiphilic molecules is represented by a bead-spring model. Neighboring beads along the molecular backbone are connected by bonded interactions that are comprised of a harmonic bond-length potential, characterized by a rest length, l_0, and spring constant, k_s, and a bond-angle term with bending stiffness, k_b. For each amphiphile these interactions take the form

$$\frac{U_b}{k_B T} = \frac{k_s}{2}\sum_{i=1}^{N-1}(r_{i,i+1} - l_0)^2 + k_b\sum_{i=2}^{N-1}(1-\cos\theta_i), \tag{A1}$$

where $r_{i,i+1} = |\mathbf{r}_{i+1} - \mathbf{r}_i|$ denotes the length of the bond between bead $i+1$ and i of the linear molecule and θ_i is the angle between vectors $\mathbf{r}_{i-1,i}$ and $\mathbf{r}_{i,i+1}$. These two terms control the molecular stiffness and the configurational fluctuations of a molecule, which is important because the average shape of a molecule depends on the curvature of the membrane.

The non-bonded interactions, that represent the repulsion of hydrophobic, A-type beads and hydrophilic head beads of types B and C, are incorporated through a third-order expansion of the non-bonded free energy in terms of local densities for each bead type

$$\frac{U_{nb}}{k_B T} = \sum_{i=1}^{n\times N}\delta_{\alpha t(i)}\left[\frac{v_{\alpha\beta}}{2N}\bar{\rho}_{2\beta}(\mathbf{r}_i) + \frac{w_{\alpha\beta\gamma}}{3N}\bar{\rho}_{3\beta}(\mathbf{r}_i)\bar{\rho}_{3\gamma}(\mathbf{r}_i)\right], \tag{A2}$$

where a summation convention is used over repeated Greek indexes $(\alpha, \beta, \gamma, t(i) \in \{A, B, C\}$, and where $t(i)$ stands for the type of bead i. The molecular weighted densities appearing in this expression are defined as

$$\bar{\rho}_{m\alpha}(\mathbf{r}) = \frac{R_{eo}^3}{N}\sum_{i=1}^{n\times N} w_m(|\mathbf{r}_i - \mathbf{r}|)\delta_{\alpha t(i)}, \tag{A3}$$

where $w_m(r)$, $m \in \{2, 3\}$ are weighting functions, and R_{eo} denotes the lipid extension. The expansion coefficients, $v_{\alpha\beta}$ and $w_{\alpha\beta\gamma}$, can be directly related to four phenomenological coefficients describing the thermodynamics of the system: the incompressibility of the hydrophobic interior, $\kappa_T N$, and its density, ρ_{coex}, the incompatibility between hydrophobic and hydrophilic beads $\chi_{th} N$, the incompatibility between different

head groups $\chi_{\rm hh}N$. This parameterization yields

$$\begin{aligned} v_{AA} &= -2\frac{\kappa_T N+3}{\rho_{\rm coex}}, \\ v_{AB} &= v_{AC} = \frac{\chi_{\rm th}N}{\rho_{\rm coex}} + \frac{v_{AA}+v_{BB}}{2}, \\ v_{BC} &= \frac{\chi_{\rm hh}N}{\rho_{\rm coex}} + \frac{v_{BB}+v_{CC}}{2}, \\ v_{BB} &= v_{CC} = 0.1, \\ w_{AAA} &= w_{AAB} = w_{ABB} = \frac{3}{2}\frac{\kappa_T N+2}{\rho^2_{\rm coex}}, \\ w_{ABC} &= w_{AAC} = w_{ACC} = \frac{3}{2}\frac{\kappa_T N+2}{\rho^2_{\rm coex}}, \\ w_{BBB} &= w_{BBC} = w_{BCC} = w_{CCC} = 0. \end{aligned} \tag{A4}$$

The set of parameters used in this simulations was adopted from Ref. 19, where a systematic study of parameter space has been performed to (i) evaluate model's capability to self-assemble into different morphologies (spherical micelles, cylindrical micelles, worm-like micelles, bilayers, or bilayers with hydrophilic inclusions) and (ii) adjust parameters to reproduce some characteristic properties of lipid bilayers, such as the density profile, elastic constants, and diffusion coefficient. Parameter values use for this study are compiled in Table III. As seen from Eq. (A4), the repulsive interaction between polar head group beads, *B* and *C*, of different lipid species is directly set by the virial coefficient v_{BC}, which, in turn, depends on the incompatibility $\chi_{\rm hh}$. This repulsion will be the leading factor contributing to the bare incompatibility, χ, of our phenomenological model (see Eq. (3)). However, there is no simple correspondence between these quantities, since χ also incorporates contributions of the repulsion between chains with similar head groups (quantified by v_{CC} and v_{BB}), the repulsion between tails and head groups in different chains (set by v_{AB} and v_{AC}), and the attraction between tails (represented by v_{AA}). In our simulations we consider two cases: *high incompatibility*, setting $v_{CB}/v_{CC} = 17$ ($\chi_{\rm hh}N = 28.8$), and *low incompatibility* case where $v_{CB}/v_{CC} = 10$ ($\chi_{\rm hh}N = 16.2$).

TABLE III. Relevant simulation parameters for the implicit-solvent model, where: $r_{\rm c}$ and τ are the length and time units, respectively, $R_{\rm eo}$ is the end-to-end (head-tail) distance of a lipid, A is the area of a planar bilayer, N is the total number of beads per lipid, $k_{\rm s}$ and l_0 are the force constant and rest length of the harmonic springs connecting beads in a single chain, $k_{\rm b}$ is the bending stiffness of the bond-angle potential, $\rho_{\rm coex}$ and κN are the density and incompressibility of the hydrophobic interior, $\chi_{\rm th}$ and $\chi_{\rm hh}$ are the hydrophobic-hydrophilic and thehydrophilic-hydrophilic incompatibilities. Δt and Υ stand, respectively, for the integration step and the thermostat collision frequency and finally, Γ is bilayer's surface tension.

Param.	Value	Param.	Value
$R_{\rm eo}$	$3.5r_{\rm c}$	A	$36.2r_{\rm c} \times 36.2r_{\rm c}$
N	16	$k_{\rm s}$	$19k_{\rm B}T/r_{\rm c}^2$
l_0	$0r_{\rm c}$	$k_{\rm b}$	$5\,k_{\rm B}T$
$\rho_{\rm coex}$	18	κN	100
$\chi_{\rm th}N$	30	$\chi_{\rm hh}N$	16.2, 28.8
Δt	0.005τ	Υ	$1.0\tau^{-1}$
Γ	$-0.5\,k_{\rm B}T/r_{\rm c}^2$		

The temperature of the system is controlled via the Lowe-Andersen thermostat,[59] where in every time step the relative velocities of all interacting pairs are randomly reassigned with probability $\Upsilon\Delta t$. The velocity update is done such that the total linear and angular momenta of the pair is conserved, i.e., the velocity component along the line passing their centers is taken from the distribution $\zeta_{ij}\sqrt{2k_{\rm B}T/m}$, where m is the mass of beads and ζ is drawn from a Gaussian distribution with zero mean and unit variance. In our simulation, we use a time step of $\Delta t = 0.005\tau$ for the Velocity-Verlet integrator and a collision frequency of $\Upsilon = 1.0\tau^{-1}$, with a time unit $\tau \equiv \sqrt{mr_{\rm c}^2/k_{\rm B}T}$.

The molecular dynamics efficiently equilibrates the molecular conformations but the redistribution of the lipids between the monolayers equilibrates very slowly because the flip-flop of lipids from one monolayer to the apposing one is protracted. To facilitate the equilibration of composition fluctuations, simulations are carried out in the semi-grand canonical ensemble,[26,60] where the total number of lipids in the system remains fixed but their concentration fluctuates around an average value fixed by the difference in chemical potential, $\Delta\mu$, between lipids. This ensemble is implemented by augmenting the molecular dynamics simulation with Monte Carlo moves, which randomly swap one lipid species into the other by changing the bead types at fixed position, with an acceptance probability

$$P_{\rm acc} = \min[1, e^{-(\Delta E \pm \Delta\mu)/k_{\rm B}T}], \tag{A5}$$

where $\Delta E = E_{\rm n} - E_{\rm o}$ is the difference in potential energy between the new (n) and old (o) configurations. The + sign in front of $\Delta\mu = \mu_C - \mu_B$ corresponds to mutating a large-head lipid to a short-head lipid, whereas the − sign applies for the reverse Monte Carlo move.

In order to enhance the effects of the curvature-composition coupling by accessing a broader range of curvatures than those naturally occurring in a tension-less bilayer, simulations have been carried out in a slightly compressed system with a surface tension $\Gamma = -0.5\,k_{\rm B}T/r_{\rm c}^2$.

In this work we consider both, simulations with planar and cylindrical bilayers. The starting configuration for the planar cases consist of a 1:1 mixture of 2340 lipids randomly distributed over each leaflet. These bilayers span over a square patch of area $A = 36.2r_{\rm c} \times 36.2r_{\rm c}$, where $r_{\rm c}$ is the cutoff radius of the non-bonded interactions. The initial configurations are equilibrated until they settle around the average composition imposed by the exchange chemical potential. Starting configurations for cylinders are constructed by a transforming and re-scaling the lipid positions from a planar bilayer into a cylinder. This procedure results in the same number of lipids but different areal densities in the two monolayers. The equilibration of monolayer densities occurs via flip-flops and is additionally facilitated by opening a pore perpendicular to cylinder's axis, as described in Appendix A 2. Typical equilibration times for planar and cylindrical configurations and for both, high and low incompatibility are on the order of 1×10^5 simulations steps, except for the particular cases with

high incompatibility and close to the demixing critical point, corresponding to $\Delta\mu = \{4.160, 4.165, 4.170\}$, for which equilibration times are on the order of 2×10^6 simulations steps. Simulation runs of $\sim 1.2 \times 10^7$ steps were required in these cases to collect enough statistics, whereas simulations away from the demixing critical point lasted $\sim 6 \times 10^6$ steps. In 10^5 steps about 2000 flip-flop movements are observed and lipid diffuses a lateral mean-squared distance of $3.64 r_c^2 \approx 0.10 \bar{1} {t_h}^2$.

2. MARTINI coarse-grained model

In addition to the minimal implicit-solvent coarse-grained model, we study the MARTINI v2.0 model.[22] In this model four heavy atoms are lumped into 1 interaction site and also water is represented by a 4-to-1 mapping. Briefly, the non-bonded interactions have Lennard-Jones and Coulomb terms, with a cut-off of 1.2 nm, and a relative dielectric constant of $\varepsilon = 15$. The bonded interactions for the lipids used in this paper are stretching and bending harmonic potentials. The unsaturated and polyunsaturated bonds in the tails are accounted for by changes in the bending parameters, the equilibrium bond angle, Θ_0, and the bending constant, K_b. In the mono-unsaturated bonds $\Theta_0 = 100^\circ$ and $K_b = 45$ kJmol^{-1} rad^{-2}, introducing an average kink in the tail, with respect to the straight saturated hydrocarbon regions ($\Theta_0 = 180^\circ$ and $K_b = 25$ kJmol^{-1} rad^{-2}. The polyunsaturated bonds are softer and with an equilibrium angle departing from 180°($\Theta_0 = 100^\circ$ and $K_b = 10$ kJmol^{-1} rad^{-2}), allowing for a looser packing and shape fluctuations. The lipids we used have a phosphatidylethanolamine (PE) or a phosphatidylcholine (PC) headgroup. Within the MARTINI model, the difference between PE and PC mimics the capability of PE to form hydrogen-bonds between neighbor PE molecules. Both head groups have two particles, one corresponding to the phosphate region and the second to the amine region. In PE, the Lennard Jones interactions between both are stronger than in PC. The MARTINI model was shown to reproduce rather accurately the properties of pure PE and PC:PE mixtures.[56]

The MARTINI simulations were performed in the canonical ensemble, using the molecular dynamics package GROMACS 4.5.5.[61] We took a time constant of 30 fs for the cylinders and 40 fs for the planar bilayers. Cylindrical membrane tubes are about 20 nm long and of varying radii, ranging from 2000 to 3200 lipid molecules. All have an equi-molar binary composition. The planar membranes have 2024 molecules and also a 1:1 ratio between the lipids. All simulations were performed at 300 K, by coupling to a Berendsen thermostat, with a relaxation time of 0.3 ps. Planar bilayers were maintained at constant volume (NVT ensemble) with an area corresponding to the tensionless state. We also run simulations at vanishing lateral membrane tension. This was achieved in GROMACS with a semi-isotropic scheme coupling to a Parrinello-Rahman barostat setting the average pressure to 1 bar in the xy plane and z directions. In this case, the lateral area $A = L_x \times L_y$ is free to fluctuate at fixed aspect ratio and, in the perpendicular direction, L_z is allowed to independently fluctuate. The masses for the equations of motions associated to the area A and L_x are parameterized in GROMACS (see Section 3.4.9 in GROMACS 4.5.5 Manual[61]) in such a way that the parameters for the coupling are given by a coupling time constant of 20 ps, and "isothermal compressibility" of $\beta_{PR} = 3 \times 10^{-5}$ bar^{-1}.

The cylindrical membranes were kept, with the same semi-isotropic Parrinello-Rahman scheme, at a fixed length of the cylinder axis, and an average pressure of 1bar perpendicular to the axis. This was achieved by setting the "isothermal compressibility" to $\beta_{PR} = 0$ in the direction of the cylinder axis, and $\beta_{PR} = 3 \times 10^{-5}$ bar^{-1} in the perpendicular direction.

This physical setting is analogous to that of pulling experiments that measure the force needed to extend a membrane tether. We opened 4 pores per cylinder to equilibrate the composition between leaflets. Lipids diffuse freely from one leaflet to the other through the pores. Pores were opened by applying a harmonic potential of the following form, $w_p = -k_p(|\mathbf{r} - \mathbf{r}_p| - R_p)^2$, where $\mathbf{r}$ is the bead position, $\mathbf{r}_p$ denotes the center of the pore, R_p is a cut-off distance that ultimately determines the pore radius, and k_p is the force constant. The potential was only applied to tail particles within the cut-off from the pore center. We defined two pore axes at $\mathbf{r_p}$ and $\mathbf{r'_p}$ along the cylinder radial direction. Each axis goes through the cylinder twice, opening a pair of pores (cf. Fig. 2). The force constant was set to $k_p = 50$ kJmol^{-1} nm^{-1} and the pore radius, R_p, was varied from 1nm to 2 nm for the smaller and the larger cylinders, respectively. The setting is analogous to that used in Refs. 62 and 63.

The equilibrium of the bilayers was determined by monitoring the composition of the monolayers. The cylinders reached its equilibrium values within the first 2.5 μs to 4.5 μs. We extended the production runs from 4 μs to 10 μs, to sample in a better way the composition fluctuations. The flow rate through each pore was of 0.1–0.25 molecules/ns. To identify a flip-flop event we followed the molecules that changed leaflet, considering only those placed at least 1 nm away from the pore edge. Based on this criteria, the total number of molecules that migrate from one leaflet to the other in the course of our simulations was at least 1.4 times the total number of molecules in the cylindrical membranes. Lipids diffused over a mean squared distance of $\sim$100 nm^2 per μs to $\sim$145 nm per μs, in the least and the most insaturated bilayers, respectively. Typical equilibration times for planar membranes were in the order of 700 ns. Production runs of around 4 μs gave good statistics for large membrane fluctuation modes, to extract the bending modulus.

Within the MARTINI model, the bilayer thickness, t_h, in Eq. (1) was defined as the distance between the PO4 residues of the outer and inner monolayers, $t_h = (R_{\text{PO4-outer}} - R_{\text{PO4-inner}})$, and the neutral surface was set at the position $R_{\text{PO4-inner}} + t_h/2$.

APPENDIX B: CURVATURE-DEPENDENT BENDING RIGIDITY

Because of symmetry reasons, we assume that the bending rigidity depends on the square of the curvature of bilayer's

midplane

$$\kappa_u = \kappa_l = \kappa_0 \left(1 + \frac{\kappa_1}{2}\mathcal{H}^2\right), \tag{B1}$$

where κ_1 quantifies the curvature dependence of the bending rigidity. With this assumption, the elastic contribution to the free energy of the bilayer, Eq. (7), is modified in the following way:

$$\frac{F_{\text{ben}}}{k_{\text{B}}T} = \frac{\kappa_u}{2} A_u \left[\left(C_0 + \frac{\sigma_{\text{m}}}{\kappa_u}\lambda\phi_u\right)^2 - 2\mathcal{H}_u\left(C_0 + \frac{\sigma_{\text{m}}}{\kappa_u}\lambda\phi_u\right)\right] + \text{similar term for subscript } l. \tag{B2}$$

Expanding this expression up to second-order terms in curvature and only considering those terms that include a composition-dependent prefactor, we obtain

$$\frac{F_{\text{ben}}}{\sigma_{\text{m}} A k_{\text{B}}T} = \eta_{\text{m}}\lambda^2\Delta\phi^2 + \lambda\Delta\phi t_{\text{h}}\mathcal{H}\left[\frac{2}{t_{\text{h}}} + C_0 + \eta_{\text{m}}\lambda\psi\right] - \frac{1}{2}\left[\frac{\kappa_1\eta_{\text{m}}\lambda^2}{{t_{\text{h}}}^2}\right]\Delta\phi^2 {t_{\text{h}}}^2\mathcal{H}^2. \tag{B3}$$

Here, $\eta_{\text{m}} = \sigma_{\text{m}}/\kappa_0$. The only difference between this expression and the linear expansion, Eq. (10), is the very last term, which vanishes for $\kappa_1 = 0$. These $\mathcal{H}^2$-corrections modify Eq. (12) resulting in

$$\begin{aligned} 0 = & -\left[\frac{\kappa_1\eta_{\text{m}}\lambda^2}{{t_{\text{h}}}^2}\right]\Delta\phi^* {t_{\text{h}}}^2\mathcal{H}^2 - \chi_{\text{eff}}\phi^* \\ & + \frac{1}{2}\ln\left[\frac{(1+\Delta\phi^*)^2 - \psi^2}{(1-\Delta\phi^*)^2 - \psi^2}\right] \\ & + t_{\text{h}}\mathcal{H}\left\{\frac{1}{4}\left[\frac{(1+\psi)^2 - \Delta\phi^{*2}}{(1-\psi)^2 - \Delta\phi^{*2}}\right] + \psi\left[\eta_{\text{m}}\lambda^2 - \frac{\chi_{\text{eff}}}{2}\right] \right. \\ & \left. + \lambda\left[\frac{2}{t_{\text{h}}} + C_0\right]\right\}, \end{aligned} \tag{B4}$$

which, in the limit of small composition differences, $|\Delta\phi^*| \ll |\Delta\phi_s|$, reduces to the analog of Eq. (13)

$$\begin{aligned} 0 = & -\left[\frac{\kappa_1\eta_{\text{m}}\lambda^2}{{t_{\text{h}}}^2}\right]\Delta\phi^* {t_{\text{h}}}^2\mathcal{H}^2 + \left[\frac{2}{1-\psi} - \chi_{\text{eff}}\right]\Delta\phi^* \\ & + t_{\text{h}}\mathcal{H}\left[\frac{1}{2}\ln\left(\frac{1+\psi}{1-\psi}\right) + \psi\left(\eta_{\text{m}}\lambda^2 - \frac{\chi_{\text{eff}}}{2}\right) \right. \\ & \left. + t_{\text{h}}\left(\frac{2}{t_{\text{h}}} + C_0\right)\right]. \end{aligned} \tag{B5}$$

For the special case of an equi-molar mixture, $\psi = 0$, we obtain

$$\Lambda_{\text{eff}} \equiv \frac{\Delta\phi^*}{\mathcal{H}} = -\frac{\lambda(2 + C_0 t_{\text{h}})}{2 - \chi_{\text{eff}} - \kappa_1\eta_{\text{m}}\lambda^2\mathcal{H}^2}. \tag{B6}$$

Since $\kappa_1 > 0$, such a consideration is in qualitative agreement with the deviations from the linear behavior in Fig. 8 but the statistical uncertainty does not warrant a quantitative analysis.

[1] T. Baumgart, B. R. Capraro, C. Zhu, and S. L. Das, Annu. Rev. Phys. Chem. **62**, 483 (2011).
[2] M. Schick, Phys. Rev. E **85**, 031902 (2012).
[3] R. Shlomovitz and M. Schick, Biophys. J. **105**, 1406 (2013).
[4] R. Shlomovitz, L. Maibaum, and M. Schick, Biophys. J. **106**, 1979 (2014).
[5] S. Sadeghi, M. Müller, and R. L. C. Vink, Biophys. J. **107**, 1591 (2014).
[6] H. T. McMahon and J. L. Gallop, Nature **438**, 590 (2005).
[7] M. Müller and M. Schick, J. Chem. Phys. **105**, 8282 (1996).
[8] K. Katsov, M. Müller, and M. Schick, Biophys. J. **90**, 915 (2006).
[9] M. Hu, D. H. de Jong, S. J. Marrink, and M. Deserno, Faraday Discuss. **161**, 365 (2013).
[10] S. M. Oversteegen and F. A. M. Leermakers, Phys. Rev. E **62**, 8453 (2000).
[11] G. Gompper and S. Zschocke, Phys. Rev. A **46**, 4836 (1992).
[12] S. Leibler and D. Andelman, J. Phys. **48**, 2013 (1987).
[13] D. Andelman, T. Kawakatsu, and K. Kawasaki, EPL **19**, 57 (1992).
[14] P. Hansen, L. Miao, and J. Ipsen, Phys. Rev. E **58**, 2311 (1998).
[15] P. B. S. Kumar, G. Gompper, and R. Lipowsky, Phys. Rev. E **60**, 4610 (1999).
[16] W. T. Gozdz and G. Gompper, EPL **55**, 587 (2001).
[17] J. L. Harden, F. C. MacKintosh, and P. D. Olmsted, Phys. Rev. E **72**, 011903 (2005).
[18] S. May, Soft Matter **5**, 3148 (2009).
[19] M. Hömberg and M. Müller, J. Chem. Phys. **132**, 155104 (2010).
[20] M. Hömberg and M. Müller, EPL **97**, 68010 (2012).
[21] M. Fuhrmans and M. Müller, Langmuir **29**, 4335 (2013).
[22] S. J. Marrink, H. J. Risselada, S. Yefimov, D. P. Tieleman, and A. H. de Vries, J. Phys. Chem. B **111**, 7812 (2007).
[23] W. Helfrich, Z. Naturforsch., C **28**, 693 (1973).
[24] A. Callan-Jones, B. Sorre, and P. Bassereau, Cold Spring Harbor Perspect. Biol. **3**, a004648 (2011).
[25] N. Fuller and R. P. Rand, Biophys. J. **81**, 243 (2001).
[26] J. de Jason, Jiang Yong, Yin Fuchang, and J. T. Kindt, J. Phys. Chem. B **110**, 25875 (2006).
[27] B. Sorre, A. Callan-Jones, J. B. Manneville, P. Nassoy, J. F. Joanny, J. Prost, B. Goud, and P. Bassereau, Proc. Natl. Acad. Sci. U. S. A. **106**, 5622 (2009).
[28] M. Rovere, D. W. Hermann, and K. Binder, EPL (Europhys. Lett.) **6**, 585 (1988).
[29] K. Kaski, K. Binder, and J. D. Gunton, Phys. Rev. B **29**, 3996 (1984).
[30] S. A. Safran, *Statistical Thermodynamics of Surfaces, Interfaces and Membranes* (Addison-Wesley, Reading MA, 1994).
[31] K. Binder, Z. Phys. B **43**, 119 (1981).
[32] N. B. Wilding and M. Müller, J. Chem. Phys. **102**, 2562 (1995).
[33] M. Müller and N. B. Wilding, Phys. Rev. E **51**, 2079 (1995).
[34] S. Joubaud, A. Petrosyan, S. Ciliberto, and N. B. Garnier, Phys. Rev. Lett. **100**, 180601 (2008).
[35] B. Zheng, Phys. Rev. E **67**, 026114 (2003).
[36] A. R. Honerkamp-Smith, S. L. Veatch, and S. L. Keller, Biochim. Biophys. Acta, Biomembr. **1788**, 53 (2009).
[37] G. van Meer, D. R. Voelker, and G. W. Feigenson, Nat. Rev. Mol. Cell Biol. **9**, 112 (2008).
[38] J. M. Seddon, G. Cevc, and D. Marsh, Biochemistry **22**, 1280 (1983).
[39] J. M. Seddon, G. Cevc, R. D. Kaye, and D. Marsh, Biochemistry **23**, 2634 (1984).
[40] P. M. Brown, J. Steers, S. W. Hui, P. L. Yeagle, and J. R. Silvius, Biochemistry **25**, 4259 (1986).
[41] V. A. Harmandaris and M. Deserno, J. Chem. Phys. **125**, 204905 (2006).
[42] H. J. Risselada, S. J. Marrink, and M. Müller, Phys. Rev. Lett. **106**, 148102 (2011).
[43] S. Baoukina, S. J. Marrink, and D. P. Tieleman, Faraday Discuss. **144**, 393 (2010).
[44] J. Zimmerberg and M. M. Kozlov, Nat. Rev. Mol. Cell Biol. **7**, 9 (2006).
[45] S. Leikin, M. Kozlov, N. Fuller, and R. Rand, Biophys. J. **71**, 2623 (1996).
[46] N. Fuller, C. R. Benatti, and R. P. Rand, Biophys. J. **85**, 1667 (2003).
[47] B. Kollmitzer, P. Heftberger, M. Rappolt, and G. Pabst, Soft Matter **9**, 10877 (2013).
[48] J. A. Szule, N. L. Fuller, and R. P. Rand, Biophys. J. **83**, 977 (2002).
[49] D. Mannock, R. Lewis, R. McElhaney, P. Harper, D. Turner, and S. Gruner, Eur. Biophys. J. **30**, 537 (2001).
[50] C. Rosetti and C. Pastorino, J. Phys. Chem. B **115**, 1002 (2011).
[51] L. Holte, F. Separovic, and K. Gawrisch, Lipids **31**, S199 (1996).
[52] H. J. Risselada and S. J. Marrink, Phys. Chem. Chem. Phys. **11**, 2056 (2009).
[53] S. L. Veatch and S. L. Keller, Biophys. J. **85**, 3074 (2003).
[54] S. R. Shaikh, M. R. Brzustowicz, N. Gustafson, W. Stillwell, and S. R. Wassall, Biochemistry **41**, 10593 (2002).
[55] C. Rosetti and C. Pastorino, J. Phys. Chem. B **116**, 3525 (2012).

[56]S.-J. Marrink and A. E. Mark, Biophys. J. **87**, 3894 (2004).
[57]K. C. Daoulas and M. Müller, Soft Matter **9**, 4097 (2013).
[58]Y. Norizoe, K. C. Daoulas, and M. Müller, Faraday Discuss. **144**, 369 (2010).
[59]C. P. Lowe, EPL (Europhys. Lett.) **47**, 145 (1999).
[60]M. Müller and K. Binder, Macromolecules **28**, 1825 (1995).
[61]D. van der Spoel, E. Lindahl, B. Hess, G. Groenhof, A. E. Mark, and H. J. C. Berendsen, J. Comput. Chem. **26**, 1701 (2005).
[62]H. J. Risselada, A. E. Mark, and S. J. Marrink, J. Phys. Chem. B **112**, 7438 (2008).
[63]Y. G. Smirnova, S. Aeffner, H. J. Risselada, T. Salditt, S. J. Marrink, M. Müller, and V. Knecht, Soft Matter **9**, 10705 (2013).